---

**Article:**
Crack, J.C. orcid.org/0000-0002-4979-1910, Amara, P. orcid.org/0000-0001-9634-7305, de Rosny, E. orcid.org/0000-0002-8197-8961 et al. (6 more authors) (2023) Probing the reactivity of [4Fe-4S] fumarate and nitrate reduction (FNR) regulator with O2 and NO: increased O2 resistance and relative specificity for NO of the [4Fe-4S] L28H FNR cluster. Inorganics, 11 (12). 450. ISSN 2304-6740

https://doi.org/10.3390/inorganics11120450

---

*inorganics*

MDPI

*Article*

# Probing the Reactivity of [4Fe-4S] Fumarate and Nitrate Reduction (FNR) Regulator with $O_2$ and NO: Increased $O_2$ Resistance and Relative Specificity for NO of the [4Fe-4S] L28H FNR Cluster

**Jason C. Crack [1], Patricia Amara [2], Eve de Rosny [2], Claudine Darnault [2], Melanie R. Stapleton [3], Jeffrey Green [3], Anne Volbeda [2], Juan C. Fontecilla-Camps [2,*] and Nick E. Le Brun [1,*]**

1 Centre for Molecular and Structural Biochemistry, School of Chemistry, University of East Anglia, Norwich NR4 7TJ, UK
2 Metalloproteins Unit, Institut de Biologie Structurale, Univ. Grenoble Alpes, CEA, CNRS, 38000 Grenoble, France
3 School of Biosciences, University of Sheffield, Sheffield S10 2TN, UK
* Correspondence: juan.fontecilla@ibs.fr (J.C.F.-C.); n.le-brun@uea.ac.uk (N.E.L.B.)

**Abstract:** The *Escherichia coli* fumarate and nitrate reduction (FNR) regulator acts as the cell's master switch for the transition between anaerobic and aerobic respiration, controlling the expression of >300 genes in response to $O_2$ availability. Oxygen is perceived through a reaction with FNR's [4Fe-4S] cluster cofactor. In addition to its primary $O_2$ signal, the FNR [4Fe-4S] cluster also reacts with nitric oxide (NO). In response to physiological concentrations of NO, FNR de-represses the transcription of *hmp*, which encodes a principal NO-detoxifying enzyme, and fails to activate the expression of the nitrate reductase (*nar*) operon, a significant source of endogenous cellular NO. Here, we show that the L28H variant of FNR, which is much less reactive towards $O_2$ than wild-type FNR, remains highly reactive towards NO. A high resolution structure and molecular dynamics (MD) simulations of the closely related L28H-FNR from *Aliivibrio fischeri* revealed decreased conformational flexibility of the Cys20-Cys29 cluster-binding loop that is suggested to inhibit outer-sphere $O_2$ reactivity, but only partially impair inner-sphere NO reactivity. Our data provide new insights into the mechanistic basis for how iron–sulfur cluster regulators can distinguish between $O_2$ and NO.

**Keywords:** FNR; gene regulation; nitric oxide sensing; iron–sulfur; molecular dynamics



**Citation:** Crack, J.C.; Amara, P.; de Rosny, E.; Darnault, C.; Stapleton, M.R.; Green, J.; Volbeda, A.; Fontecilla-Camps, J.C.; Le Brun, N.E. Probing the Reactivity of [4Fe-4S] Fumarate and Nitrate Reduction (FNR) Regulator with $O_2$ and NO: Increased $O_2$ Resistance and Relative Specificity for NO of the [4Fe-4S] L28H FNR Cluster. *Inorganics* **2023**, *11*, 450. https://doi.org/10.3390/inorganics11120450

Academic Editor: Nunziata Maio

Received: 27 September 2023
Revised: 31 October 2023
Accepted: 15 November 2023
Published: 21 November 2023



## 1. Introduction

Iron–sulfur cluster-containing transcriptional regulators comprise a growing family that control a range of key cellular pathways, such as aerobic and anaerobic respiration, iron–sulfur cluster biogenesis, iron uptake and responses to oxidative and nitrosative stress [1,2]. In all cases, the cluster functions as the sensory module, but information about sensing mechanisms has been difficult to obtain because of the sensitivity of such proteins to aerobic conditions [2]. One of the best studied iron–sulfur cluster regulators is the homodimeric fumarate and nitrate reduction (FNR) regulator from *Escherichia coli* (*Ec*), a member of the large CRP-FNR protein family, which directly senses $O_2$ and, through this, controls the switch between aerobic and anaerobic respiration [3–8].

While the structure of *Ec*FNR is not yet available, the Grenoble group has reported the crystal structure of *Aliivibrio fischeri* (*Af*) FNR, which regulates the $O_2$-dependent luciferin–luciferase bioluminescence reaction and the anaerobic respiration of this symbiont in the light organ of several marine organisms [9–11]. Similarly to other members of the CRP-FNR protein family, each FNR monomer has two domains that, respectively, function in signal sensing and DNA-binding functions. However, its mechanism of transcriptional regulation is fundamentally different to other characterized members of the family. In the

absence of $O_2$, the N-terminal sensory domain coordinates a $[4Fe\text{-}4S]^{2+}$ cluster through four Cys residues (Cys20, 23, 29 and 122) [6,11–14]. In this state, the protein forms a homodimer and displays high-affinity, site-specific DNA binding to target promoters [4,11,15]. Under aerobic conditions, the increased levels of $O_2$ directly degrade the $[4Fe\text{-}4S]^{2+}$ cluster, leading to its conversion, via a $[3Fe\text{-}4S]^{1+}$ intermediate, into a $[2Fe\text{-}2S]^{2+}$ form [16,17]. The Norwich group has reported time-resolved electrospray ionization mass spectrometry studies of the *Ec*FNR $O_2$-dependent cluster degradation process, providing novel insight into the reaction through the simultaneous detection of already known cluster conversion intermediates and products, including the $[3Fe\text{-}4S]^{1+}$ cluster, and persulfide-coordinated $[2Fe\text{-}2S]^{2+}$ clusters ($[2Fe\text{-}2S](S)_n$, where $n$ = 1 or 2), as well as previously unrecognized intermediates such as a [3Fe-3S] cluster [18]. Importantly, changes within the cluster trigger a conformational rearrangement in the protein framework that leads to the dissociation of the protein into monomers, resulting in the loss of high-affinity, sequence-specific DNA binding [4,6,15,19].

Enteric bacteria like *E. coli*, which can respire in the absence of $O_2$ by using nitrate/nitrite as terminal electron acceptors, can produce NO endogenously [20]. They will also encounter exogenous NO generated as part of the host defense mechanisms [21]. The Norwich/Sheffield groups have previously reported that *Ec*FNR, as well as responding to $O_2$, can also respond to exogenous and endogenous sources of nitric oxide (NO) in vivo [22,23], and the in vitro response of [4Fe-4S] to NO has also been characterized in some detail [24]. Reactivity with NO in vivo is most likely limited to circumstances where exogenous or endogenous NO is present at high concentrations, because actions initiated by other dedicated NO-sensing regulatory proteins, NsrR and NorR, result in NO detoxification [24–27].

Iron–sulfur regulatory proteins that function as NO sensors are typically less sensitive to $O_2$ than FNR [25,28]. Thus, the responses to $O_2$ and NO of iron–sulfur clusters appear to have evolved to be optimal for the particular function of the regulator. However, what controls the relative sensitivities to these gases, and therefore the specificity, is not clear. Determining this is fundamental to understanding what makes one regulator primarily an NO sensor and another an $O_2$ sensor, and potentially how sensing functions could be modulated through protein engineering.

Several site-directed variants of *Ec*FNR exhibiting impaired reactivity with $O_2$ have been previously identified, including S24F [29] and L28H [30]. The S24F substitution resulted in a three-fold reduction in the rate constant for the initial reaction with $O_2$, leading to a significant increase in FNR activity under aerobic conditions [29]. L28H-*Ec*FNR exhibited an even greater $O_2$ resistance, with very little cluster degradation observed even after a 60 min exposure to $O_2$ [30]. Here, we report the crystal structure of the closely related L28H-*Af*FNR and show that it also displays high resistance to $O_2$.

As a step towards understanding the factors that control cluster reactivity and specificity, we wished to determine whether a substitution that dramatically affects $O_2$ reactivity has any effect on NO reactivity. Detailed kinetic and thermodynamic investigations of the L28H-*Ec*FNR reaction with NO reveal that, despite the presence of an $O_2$-resistant [4Fe-4S] cluster, the protein undergoes a rapid, multi-step reaction with NO, similar to that of the wild-type (wt) FNR protein [24]. In addition, molecular dynamics (MD) simulations using the [4Fe-4S] L28H-*Af*FNR crystal structure as a starting model show that the formation of a His28-Arg184 cation–$\pi$ interaction reduces the flexibility of the Cys20-Cys29 cluster-binding loop relative to the corresponding loop in the wt protein. Our results suggest how the specificity required for a reaction with the small activator molecules, $O_2$ and NO, may be modulated.

## 2. Experimental Section

### *2.1. Purification of EcFNR Proteins*

GST-FNR fusion proteins were overproduced in aerobically grown *E. coli* BL21λDE3 harboring pGS572 (wt *Ec*FNR) or pGS2251 (L28H-*Ec*FNR), which was created through site-directed mutagenesis using the Quikchange (Agilent, Santa Clara, CA, USA) protocol, with

pGS572 as the template and the mutagenic primers (5′-TGCAGCATCAGCCAGCATTGCAT CCCGTTCACACTC-3′; 5′-GAGTGTGAACGGGATGCAATGCTGGCTGATGCTGCA-3′), followed by the sequencing of the gene to confirm the mutation. The proteins were purified, cleaved to remove GST using thrombin and the [4Fe-4S] cluster was reconstituted, in vitro, as previously described [16]. The protein concentrations [31], iron/sulfide contents [28,32] and cluster loading of FNR proteins [16] were determined as previously described.

### *2.2. Purification of AfFNR Proteins*

The L28H variant of *Af*FNR was prepared through site-directed mutagenesis following the QuikChange® strategy, using *p*Strep*Af*FNR [11] as a template with the following primers: 5′-GTAGCATTTCTCAGCACTGTATCCCGTTCACC-3′; 5′-GGTGAACGGGATAC AGTGCTGAGAAATGCTAC 3′ and Phusion™ polymerase. The mutation was verified by sequencing the entire gene. Wild-type and L28H-*Af*FNR proteins were anaerobically overproduced and purified, as previously described for the wt protein [11]. The purified proteins were stored at 4 mg/mL in 50 mM Tris, pH 8.0, 300 mM NaCl and 2 mM DTT.

### *2.3. Crystallization and X-ray Structure Solution of L28H-AfFNR*

A protein sample was exposed to air for 5 min before being transferred to an anaerobic glove box for its crystallization. Brown crystals were obtained in hanging drops by mixing 1 µL of this sample with 1 µL of the crystallization solution containing 13% 2-methyl-2,4-pentanediol (MPD) in 100 mM HEPES, pH 7.1. After 20 days, the crystals were flash-cooled in a cryo-protecting solution composed of 70% MPD in 100 mM HEPES, pH 7.1, and stored in liquid $N_2$. Diffraction data were measured at 100 K to a maximum resolution of 2.40 Å for the best crystal, using an X-ray wavelength of 0.9677 Å at beamline ID23-1 of the European Synchrotron Radiation Facility in Grenoble, France. The data collection statistics after processing with XDS [33] and Aimless [34] are given in Table S1. The crystal structure was solved by molecular replacement with Phaser [35] using the coordinates of the deposited structure of wt *Af*FNR (pdb code 5E44) [11]. Next, Refmac [36] and Phenix [37] were used for rigid body, positional and temperature factor refinement. Further model improvement was obtained via manual corrections using Coot [38]. The refinement statistics are included in Table S1.

### *2.4. Spectroscopy*

UV–visible absorbance and CD data were acquired using a Jasco V500 spectrometer (Jasco UK Ltd., Heckmondwike, UK) and a Jasco J810 spectropolarimeter, respectively. EPR spectra at the X-band were acquired using a Bruker EMX spectrometer (Bruker UK Ltd., Coventry, UK) equipped with an ESR-900 helium flow cryostat (Oxford Instruments, Abingdon, UK). The quantification of the paramagnetic species was carried out using a Cu(II) EDTA standard, as previously described [24].

### *2.5. Rapid Reaction Kinetics of FNR Proteins*

*Ec*FNR: UV–visible stopped-flow experiments were performed using an Applied Photophysics (Leatherhead, UK) Bio-Sequential DX.17 MV spectrophotometer and the data were analyzed as previously described [24,39]. Prior to use, the stopped-flow system was flushed with ~30 mL of anaerobic buffer and wt FNR was used to used to confirm the absence of residual $O_2$ [40].

Wild-type and L28H-*Af*FNR: Experiments were performed using a Biologic SFM-3000/S and MOS-200 rapid kinetics spectrometer installed in a glove box. Anaerobically purified protein at 72 µM in 50 mM Tris and 300 mM NaCl, pH 8.0, without a reducing agent, was mixed in a 1:1 volume ratio with the same buffer previously exposed to air. A flow rate of 16 mL/s was used for mixing to a final volume of 150 µL; absorbance changes were detected at 420 nm with a path length of 1.5 mm.

### 2.6. Mass Spectrometry

Liquid chromatography–mass spectrometry (LC-MS) [24] and native mass spectrometry (native MS) [18] were performed as previously described.

### 2.7. Electrophoretic Mobility Shift Assays (EMSAs)

Band shift reactions (20 µL) were carried out inside a glove box in 20 mM Tris 5% (*v*/*v*) glycerol and 127 mM DTT, pH 8.0, as previously described [25]. The DNA probe contained a copy of the *napF* FNR binding site, TTTGATCCAAATCAA (site underlined), and was labelled with rhodamine green at the 5′ end (a kind gift from Prof Michael McArthur, Norwich Medical School, UEA). Briefly, 1 µL of the DNA probe was titrated with aliquots of L28H-*Ec*FNR (20 µL final volume), typically to a 30-fold molar excess, and incubated at the ambient anaerobic glove box temperature for ~10 min. Outside the glove box, loading dye (2 µL, containing 0.003% (*w*/*v*) Bromophenol blue) was added and the reaction mixtures immediately separated at 30 mA for 15 min on a polyacrylamide gel (5% (*w*/*v*) upper section and a 7.5% (*w*/*v*) lower section) in 1 × TBE (89 mM Tris, 89 mM boric acid, 2 mM EDTA), using a Mini Protean III system (BioRad). The gels were visualized ($Ex_{488\,nm}$, $Em_{530\,nm}$) on a Typhoon molecular imager (Cytiva). The polyacrylamide gels were pre-run at 30 mA for 2 min prior to use. For the aerobic EMSA analysis, an aliquot (3 µL) of L28H-*Ec*FNR was removed from the glove box and exposed to air for ≥2 h at room temperature before use.

### 2.8. Other Analytical Methods

Stock solutions of the NO donor PROLI-NONOate ($t_{1/2}$ = 1.5 s; Cayman Chemicals) [41,42] were prepared and used as previously described [24]. Elemental sulfur ($S^0$) analyses [28] and gel filtration [24] were performed as previously described.

### 2.9. Molecular Dynamics (MD) Simulations of wt and L28H-AfFNR

Model setup: All calculations were performed with the Schrödinger suite [43]. Our starting models were (i) a further refined wt structure (from PDB code 5E44 [11]) and (ii) the [4Fe-4S] L28H-*Af*FNR crystal structure (this work). All hydrogen atoms were constructed and the protonation states of each residue were optimized using the Protein Preparation Protocol. In the Schrödinger suite, regardless of the force field chosen, the charges of [Fe-S] clusters are formal, i.e., +2 or +3 for the Fe atoms and −2 for the inorganic S atoms connecting them. We know from an extensive quantum study on [4Fe-4S] clusters [44] that the actual charges on the Fe atoms and the inorganic S atoms are greatly reduced due to covalency [44]. Accordingly, we modelled the [4Fe-4S] cluster in its oxidized form with a total charge of +2, and we used charges of +0.4 and −0.4 for the Fe atoms and the inorganic S atoms, respectively. Since the [4Fe-4S] cluster charges now add up to 0, the +2 charge was equally distributed, modifying the force field charges of the Cys thiolate ligands of the cluster. The OPLS4 force field [45] was employed. Our models were neutralized by adding $Na^+$ ions and further solvated with a periodically replicated orthorhombic water box using the TIP4P water model [46]. To give a theoretical salt concentration of 150 mM, additional $Na^+$ and $Cl^-$ ions were added. The resulting systems consisted of approximately 75,000 atoms.

In these models, Cys residues 20, 23 and 29 coordinate the [4Fe-4S] cluster, and each thiolate sulfur atom is bonded to an Fe atom in the force field, which strongly constrains the dynamics of the Cys20-Cys29 loop. Since we wanted to compare the intrinsic dynamics of the loop of wt and L28H-*Af*FNR, we constructed two additional models of wt and L28H-*Af*FNR, without the [4Fe-4S] cluster, and we protonated the four Cys thiolate groups.

MD simulations: The Desmond program [47] included in the Schrödinger suite was used for all molecular dynamics simulations. The default protocol was used to equilibrate the system and heat it from 0 to 300 K. The simulations of the wt and the [4Fe-4S] L28H-dimer models were then run for 1 µs with a time step of 2 fs in the isobaric, isothermal (NPT) ensemble, with a temperature of 300 K and a pressure of 1 atm. The Cys20-Cys29

loop dynamics were analyzed in chains A and B for both models. To evaluate whether the cation–π interaction between Arg184 and His28 can occur in the [4Fe-4S] and apo L28H-*Af*FNR proteins, the simulated trajectories were analyzed, calculating the radial distribution functions (RDF) between the Cζ atom of Arg184 and the center of mass of the imidazole ring of His28. The same type of trajectory analysis was performed for Arg184 and Leu28 to check whether the two residues kept the van der Waals interaction observed in the crystal.

## 3. Results

### *3.1. Spectroscopic, $O_2$ Reactivity and DNA-Binding Properties of [4Fe-4S] L28H-EcFNR*

The purification of L28H-*Ec*FNR resulted in a brown solution that gave UV–visible and CD spectra that are not only characteristic of a [4Fe-4S] cluster, but also almost identical to those of wt-*Ec*FNR [16] (Figure 1). Iron and sulfide analyses of the as-isolated protein revealed a cluster incorporation level of ~60% (Table 1). Similar observations were made via Mössbauer [30]. Thus, spectroscopic techniques that are highly sensitive to the cluster environment indicated that the replacement of Leu28 by His did not result in any significant structural changes in the *Ec*FNR cluster.

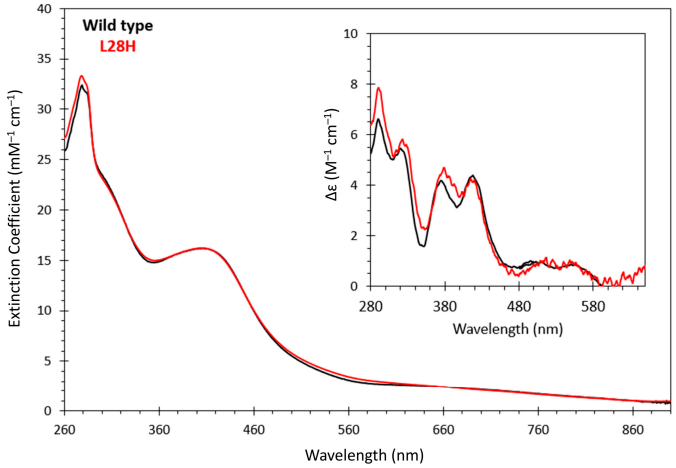


**Figure 1.** Spectroscopic characterization of [4Fe-4S] L28H-*Ec*FNR. UV–visible absorbance spectra and circular dichroism (CD) spectra (inset) of [4Fe-4S] L28H (red line) and wild-type (black line) *Ec*FNR proteins. The sample buffer was 25 mM HEPES, 2.5 mM $CaCl_2$, 100 mM NaCl and 100 mM $NaNO_3$, pH 7.5.

**Table 1.** Sulfide ($S^{2-}$) and sulfur ($S^0$) content of NO-treated [4Fe-4S] L28H-*Ec*FNR.

| | | | Before Treatment with NO | | After Treatment with NO (~530 µM) [a] | | | |
|---|---|---|---|---|---|---|---|---|
| **Sample** | **Conc/ µM** | **[4Fe-4S]/ µM** | **$S^{2-}$/ µM [a]** | **$S^{2-}$/ [4Fe-4S]** | **$S^{2-}$/ µM** | **$S^{2-}$/ [4Fe-4S]** | **$S^0$ /µM** | **$S^0$/ [4Fe-4S]** |
| 1 | 44.2 | 25.3 | 101.12 (±3.00) | 4.00 (±0.12) | 23.79 (±0.73) | 0.94 (±0.03) | 96.94 (±11.46) | 3.84 (±0.45) |
| 2 | 62.9 | 36.0 | 143.80 (±4.26) | 4.00 (±0.12) | n.d. | n.d. | 108.89 (±10.14) | 3.03 (±0.28) |
| 3 [b] | 40.3 | 23.0 | 92.20 (±2.73) | 4.00 (±0.12) | 2.76 (±0.00) | 0.12 (±0.00) | 53.33 (±5.01) | 2.31 (±0.22) |

[a] Samples treated with ~15-fold excess of NO over cluster. [b] Samples were gel-filtered (PD10, Cytiva) to remove any low-molecular-weight species.

The L28H substitution greatly stabilizes the [4Fe-4S] cluster against $O_2$ exposure [30]. The reactivity of our L28H-*Ec*FNR preparations with $O_2$ was analyzed using native mass

spectrometry. Previous studies of *Ec*FNR have revealed a series of cluster conversion intermediates formed upon reaction with $O_2$. For L28H, the cluster reactivity was, as expected, much lower, and intermediates were not readily detected (Figure S1A). After 140 min, the [4Fe-4S] form was still present, and while [2Fe-2S] and [2Fe-2S](S) forms were detected, these were very low-intensity. The major species detected was apo protein and its persulfide adducts, containing up to three additional persulfides (Figure S1A).

To analyze the effect of the impaired $O_2$ sensitivity of the [4Fe-4S] cluster on site-specific DNA binding, electrophoretic mobility shift assays using probes containing the *napF* FNR recognition site (TTGAT-$(n)_x$-ATCAA) were carried out. As previously reported [30], L28H-*Ec*FNR readily formed a protein–DNA complex, even in the presence of $O_2$, consistent with its ability to activate transcription in vivo under aerobic conditions [30,48]. Increases in the concentration of this variant resulted in a clear shift in the mobility of the probe (Figure 2A), and full binding was achieved at a ratio of ~3 to 4 protein dimers (~6 to 8 [4Fe-4S] clusters) per FNR binding site. At ratios greater than ~5 dimers per probe, non-specific DNA interactions appeared to dominate (Figure 2A).

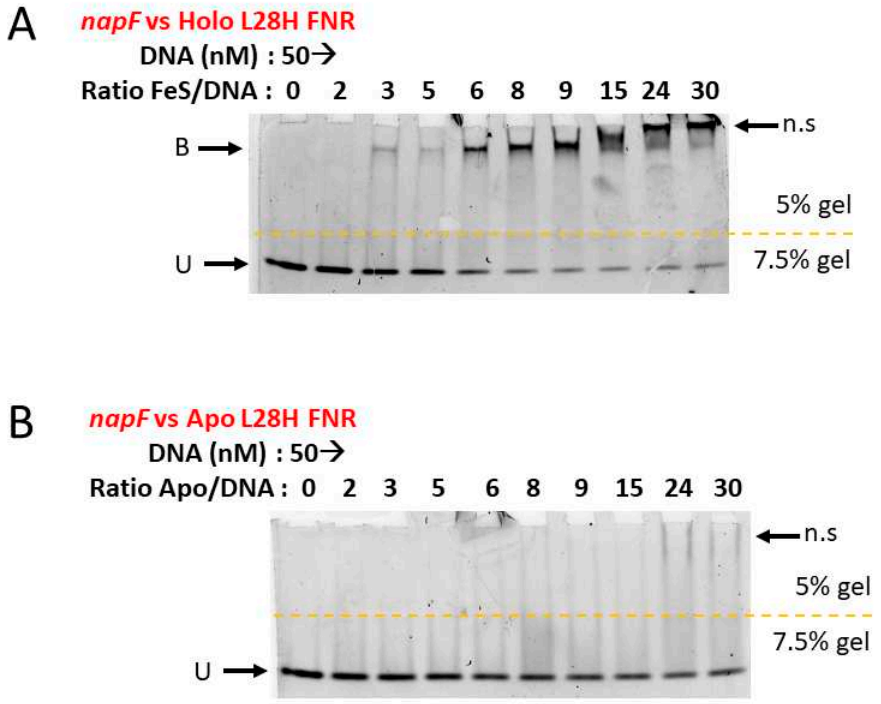


**Figure 2.** DNA-binding characteristics of L28H-*Ec*FNR. DNA-binding EMSAs with (**A**) holo L28H-*Ec*FNR (81% [4Fe-4S] loading) and (**B**) apo L28H-*Ec*FNR. The labelled *napF* FNR binding site (50 nM) was incubated with either holo or apo L28H-*Ec*FNR at the indicated ratios. U, unbound DNA probe; B, specifically bound DNA probe; n.s., non-specifically bound DNA probe. The location of the change in the polyacrylamide composition of the gel is indicated by the dashed yellow line.

To determine whether the DNA binding was cluster-specific, an L28H-*Ec*FNR solution was exposed to $O_2$ until colorless. We note that, despite its enhanced $O_2$ tolerance, the variant did eventually succumb to the effects of this gas. This apo form of L28H-*Ec*FNR failed to bind to the *napF* DNA target (Figure 2B). These EMSA observations are consistent with previously reported DNA binding for [4Fe-4S] wt and L28H-*Ec*FNR [30] and confirm that the integrity of the cluster is essential for the DNA binding of both proteins.

### *3.2. [4Fe-4S] L28H-EcFNR Reacts with Multiple NO Molecules*

L28H-*Ec*FNR was previously shown to react with $O_2$ much more slowly than the wt cluster, both in vitro and in vivo [30]. Thus, it remains transcriptionally active in the cell under aerobic conditions. The $O_2$ sensitivity of the L28H-*Ec*FNR preparations used here

was as previously reported [30]. In order to gain novel insight into iron–sulfur cluster reaction specificity, the NO reactivity of this variant was also investigated.

Sequential additions of NO to an anaerobic sample of L28H-*Ec*FNR were followed by UV–visible absorbance spectroscopy (Figure 3A). The changes observed included a decrease in $A_{406\ nm}$, an increase in $A_{360\ nm}$ and a lesser increase at $A_{500\ nm}$–$A_{700\ nm}$, indicating the formation of iron–nitrosyl species [24,28]. Isosbestic points were apparent at 295, ~390 and ~640 nm, and a plot of changes at $A_{360\ nm}$ as a function of NO per cluster gave an almost linear response, with a slight inflection point at a ~4 [NO]:[4Fe-4S] ratio and a reaction end point of 8–9 NO molecules per cluster (Figure 3B). Changes at 406 nm were linear and saturated at ~8 NO molecules per cluster (Figure 3B). A similar titration experiment was conducted using near-UV–visible CD, where signals arising from the [4Fe-4S] cluster decreased in intensity, essentially to zero, as the reaction with NO advanced (Figure 3C). The plot of the CD intensity at 418 nm as a function of [NO]:[4Fe-4S] was linear and indicated the completion of the reaction at ~8 NO molecules per cluster (Figure 3B).

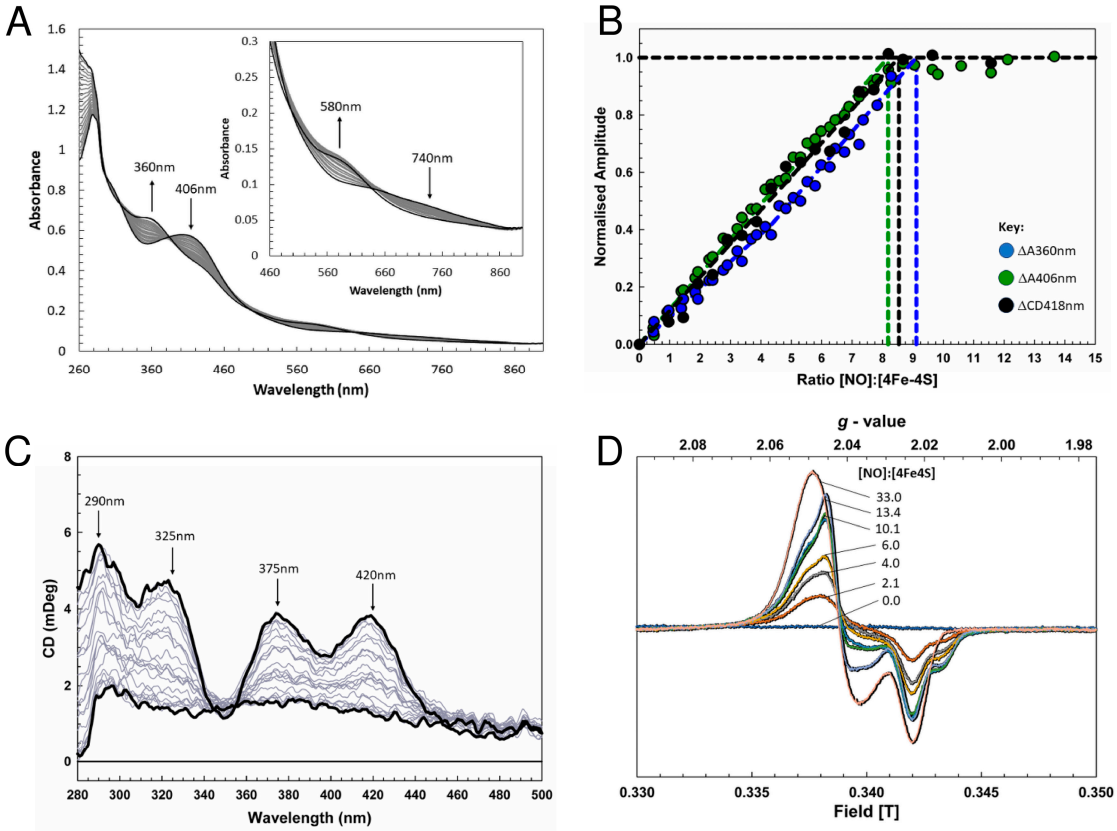


**Figure 3.** Reaction of [4Fe-4S] L28H-*Ec*FNR with NO. (**A**) Absorbance spectra of [4Fe-4S] L28H-*Ec*FNR (35.7 μM) following sequential additions of NO up to a 12-fold excess over the [4Fe-4S] cluster. (**B**) $\Delta A_{360\ nm}$ (blue circles), $\Delta A_{406\ nm}$ (green circles) and $\Delta CD_{418\ nm}$ (black circles) were normalized and plotted against the ratio of [NO] to the [4Fe-4S] cluster. Tangents to the initial slope and the end point plateau regions of the absorbance and CD data are drawn in and the points of intersection are marked. (**C**) CD spectra resulting from a titration equivalent to that in (**A**). Spectra recorded at the beginning and end of the titration are in black; intervening spectra are in gray. (**D**) EPR spectra recorded at 74 K following the addition of NO to 33.8 μM [4Fe-4S] L28H-*Ec*FNR at [NO] to [4Fe-4S] ratios of 0.0, 2.1, 4.0, 6.0, 8.3, 10.1, 13.4 and 33.0. The line shapes are characteristic of more than one S = 1/2 species, as observed previously. The microwave power and frequency were 2 mW and 9.68 GHz, respectively, and the field modulation amplitude was 1 mT. Arrows indicate the direction of spectral changes.

Although the L28H-*Ec*FNR cluster is spectroscopically indistinguishable from that of the wt *Ec*FNR, its reaction with NO showed some important differences. While the reaction of the wt protein was also complete at a level of 8–9 NO molecules per cluster, both absorbance and CD measurements indicated the formation of a stable intermediate at ~4–5 NO molecules per cluster. Furthermore, the absorbance titration data plot did not contain any isosbestic points [24]. Thus, the L28H-*Ec*FNR reaction with NO exhibited distinct behavior in the evolution of intermediates and products compared to the wt protein. However, despite these differences, the final spectral form and intensity were similar for both proteins.

The titration of [4Fe-4S] L28H-*Ec*FNR with NO under conditions identical to those above was monitored using EPR spectroscopy (Figure 3D; Figure S2). Complex signals centered on g ≈ 2.03 were observed, similar to those previously reported for wt nitrosylated *Ec*FNR in vivo [49] and in vitro [24]. The spectra were deconvoluted to reveal contributions from three distinct di-nitrosyl iron complexes (DNICs), S = $\frac{1}{2}$ species (see Figure S2), including a sharp feature at g ≈ 2.04 ($g_{\perp}$ = 2.044, $g_{=}$ = 2.032) that is similar to that previously assigned as an FNR-associated persulfide ligated DNIC [50]. The quantification of the DNIC signals gave a concentration corresponding to ~26% of the original cluster (~6% of the original iron). Thus, the majority of the iron was EPR silent. This, together with the optical changes (with bands at 310 and 360 nm), indicated that diamagnetic multi-nuclear iron nitrosyl species, such as Roussin's Red Ester-like species, are the major product(s) (see below).

The gel filtration of [4Fe-4S] L28H-*Ec*FNR before and after the addition of NO gave masses of 54 kDa and 37 kDa, respectively (Figure S3). Although the variant has an actual mass of ~29 kDa, wt *Ec*FNR was previously shown to elute from a gel filtration column at ~30 kDa following a reaction with $O_2$ [24,51]. The UV–visible spectrum of the protein following gel filtration clearly demonstrated that the iron–nitrosyl species generated were retained by the protein (Figure S4). Thus, nitrosylation resulted in the monomerization of the protein. Again, this behavior is similar to that observed for wt *Ec*FNR [24].

### *3.3. [4Fe-4S] L28H-EcFNR Reacts Rapidly with NO*

Stopped-flow absorbance was used to follow the reaction of L28H *Ec*FNR with excess NO. Changes at 360 and 420 nm were measured, corresponding to the maxima of the final nitrosylated product and the initial iron–sulfur cluster, respectively (Figure 4A,B). The data were similar to those previously reported for wt *Ec*FNR in that three distinct kinetic phases were observed at both wavelengths. While this suggested that there are three steps in the overall reaction, fitting the $A_{360\,nm}$ and $A_{420\,nm}$ data to exponential functions separately and simultaneously (Figure 5A,B) demonstrated that the middle phase has quite different kinetic characteristics at the two wavelengths. Similar observations were previously made for wt *Ec*FNR [24], *Steptomyces coelicolor* WhiD and *Mycobacterium tuberculosis* WhiB1 [28]. Thus, the middle phases at 360 nm and 420 nm must report on different processes, and so the overall reaction must consist of at least four steps, i.e., A → B → C → D → E. Steps A → B and D → E were detected at both wavelengths and correspond to the initial reaction with NO and the formation of the final product(s), respectively. Step B → C was detected at 360 nm and step C → D at 420 nm.

Compared to wt *Ec*FNR, the amplitude of $\Delta A_{420\,nm}$ corresponding to step D → E for L28H-*Ec*FNR was significantly greater, consistent with the difference in the thermodynamic titrations. The wt *Ec*FNR data indicated an intermediate species formed at ~4–5 NO molecules per cluster, with relatively little change at 420 nm at higher NO ratios. In contrast, L28H-*Ec*FNR underwent a more concerted reaction with no evidence of stable intermediates.

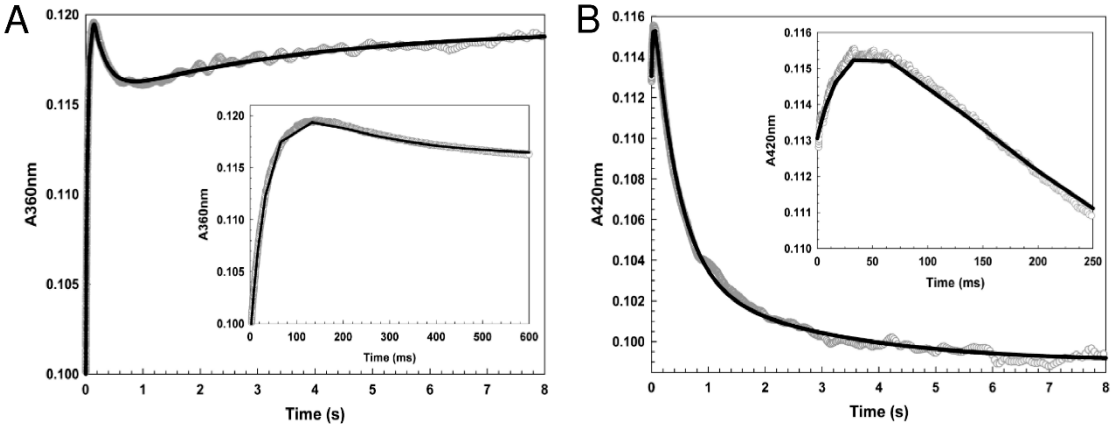


**Figure 4.** Stopped-flow measurements of the reaction of [4Fe-4S] L28H-*Ec*FNR with NO. (**A**) $A_{360\ nm}$ traces for L28H-*Ec*FNR (~7.6 μM) following the addition of NO (297 μM, an excess of [NO] over [4Fe-4S] cluster of ~39). Protein was in 25 mM HEPES, 2.5 mM $CaCl_2$, 100 mM NaCl and 100 mM $NaNO_3$, pH 7.5. (**B**) As for (**A**), except that the wavelength was 420 nm. Fits to each of the observed phases in (**A**,**B**) are drawn in black lines, and insets show early events in the reaction time course.

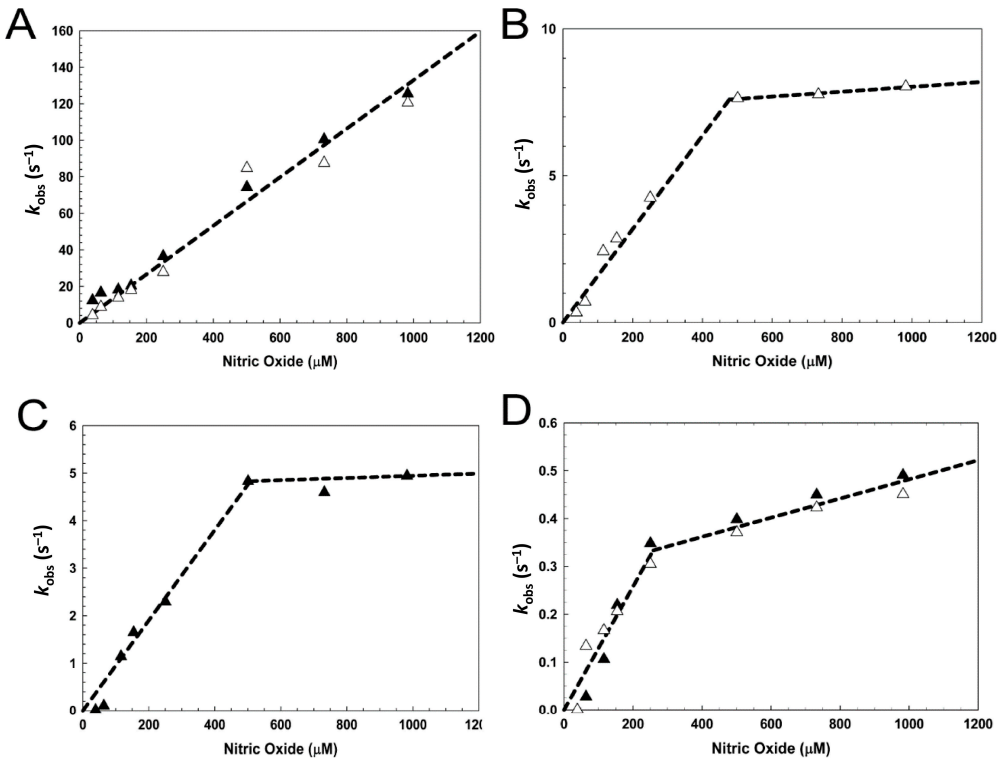


**Figure 5.** Dependence of each step of the L28H-*Ec*FNR nitrosylation reaction on NO. Stopped-flow kinetic measurements following the addition of excess NO to [4Fe-4S] L28H-*Ec*FNR (~7.6 μM) with variable excess NO were performed. The panels (**A**–**D**) correspond to steps 1–4 of the overall reaction (see main text for details), respectively, with observed (pseudo-first-order) rate constants ($k_{obs}$) obtained from fits of the kinetic data at 360 and 420 nm plotted against the NO concentration. Rate constants derived from data at $A_{360\ nm}$ are shown as white triangles, and those from $A_{420\ nm}$ as black triangles. Least-squares linear fits are shown as black dashed lines, the gradients of which correspond to the apparent second-order rate constants (see Table S2). Proteins were in 25 mM HEPES, 2.5 mM $CaCl_2$, 100 mM NaCl and 100 mM $NaNO_3$, pH 7.5.

Plots of the observed pseudo-first-order rate constants ($k_{obs}$) as a function of the NO concentration for L28H-*Ec*FNR were linear for each step at low NO concentrations,

indicating a first-order dependence on NO (see Figure 5 and Table S2). While the rate constant for the initial reaction of L28H-*Ec*FNR with NO is ~50% lower, overall, the rate constants for each step are of the same order of magnitude as those previously observed for wt *Ec*FNR [24], and also for Wbl proteins [28] (Table S2). The rate constant plots for the L28H variant protein corresponding to steps B → C → D → E exhibited quite different behavior at NO concentrations above ~250–400 μM, depending on the step. The dependence of the pseudo-first-order rate constant on NO is much less steep at high NO concentrations, suggesting that the rate-limiting process for these steps at higher NO concentrations is a different reaction, most likely not NO-binding. Overall, despite these differences in rate dependence at high NO concentrations, the kinetics of the reaction with NO were broadly similar in both the $O_2$-resistant and wt proteins.

### *3.4. Nitrosylation of L28H-EcFNR Results in Cluster Sulfide Oxidation and Formation of Protein-Associated Persulfides*

The formation of iron–nitrosyls from a $[4Fe\text{-}4S]^{2+}$ cluster requires electrons. Depending on the precise nature of the iron–nitrosyl products, up to six electrons are needed [2]. These can be obtained from cluster sulfide oxidation to generate sulfane ($S^0$), which often results in protein cysteine persulfides (-S-$S^-$), as previously shown for WhiD [28] and wt *Ec*FNR [24]. After a reaction with excess NO, L28H-*Ec*FNR contained ~0.9 $S^{2-}$ and ~3.4 $S^0$ per [4Fe-4S] cluster (Table 1), demonstrating that $S^0$ is generated via the oxidation of $S^{2-}$ [28]. Importantly, when L28H-*Ec*FNR was exposed to excess NO and subsequently passed down a gel filtration column, there was ~2 $S^0$ per cluster, but very little $S^{2-}$ remained associated with the protein (Table 1).

Protein-associated cysteine persulfides/polysulfides can be detected via LC-MS [52,53], thus providing a means to directly detect $S^0$ associated with L28H-*Ec*FNR following nitrosylation. The mass spectrum of [4Fe-4S] L28H-*Ec*FNR contained a monomer peak at 29,187 Da (theoretical mass of 29,189 Da), but also additional low-intensity peaks at intervals of +32 Da, corresponding to apo L28H-*Ec*FNR with between 1 and 4 $S^0$ adducts per protein (Figure 6).

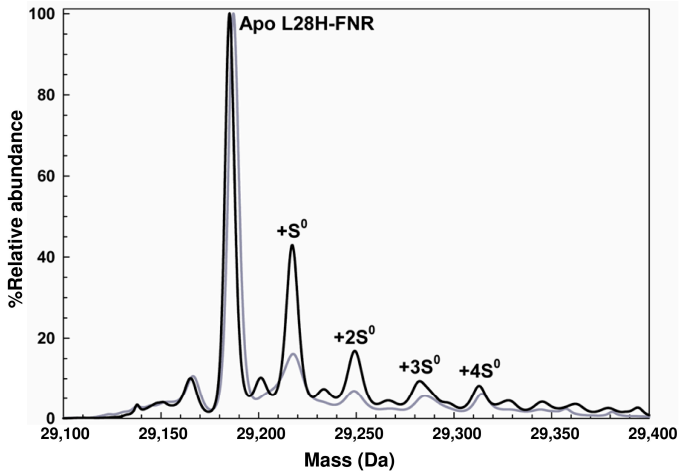


**Figure 6.** Mass spectrometric detection of persulfide species of L28H EcFNR. Deconvoluted mass spectrum of [4Fe-4S] L28H-*Ec*FNR (855 nM) before (gray line) and after (black line) the addition of NO. The highest intensity peak, at 29,187 Da, corresponds to monomeric apo L28H-*Ec*FNR, and the peaks annotated as $+S^0$, $+2S^0$, $+3S^0$ and $+4S^0$ correspond to apo protein containing up to four covalently bound sulfur atoms at +32, +64, +96 and +128 Da relative to the apo protein.

The exposure of this protein to NO prior to MS resulted in a significant increase in $S^0$ adducts, principally, one or two $S^0$ species per FNR molecule. Previous studies of wt *Ec*FNR revealed similar behavior [24], and showed that $S^0$ is also generated through the reaction with $O_2$, resulting in a persulfide that coordinates the [2Fe-2S] cluster [53]. Therefore, the

$S^0$ adduct species formed in *Ec*L28H-FNR through the action of NO are also likely to be involved in the coordination of the iron–nitrosyl core.

### *3.5. Crystal Structure and $O_2$ Reactivity of [4Fe-4S] L28H-AfFNR*

Overall, the 2.4 Å resolution L28H-*Af*FNR structure (Figure 7A) is very similar to that of the wt protein [11]. In spite of a 5 min air exposure at room temperature before crystallization, the [4Fe-4S] cluster site was fully occupied, consistent with the high $O_2$ tolerance of this variant. Low $O_2$ reactivity was also confirmed for L28H *Af*FNR via stopped-flow absorbance (Figure S5) and through native MS (Figure S1B). For the latter, and as for L28H *Ec*FNR (Figure S1A), intermediates of cluster conversion were not readily detected, with apo protein and persulfide adduct forms being the major species observed.

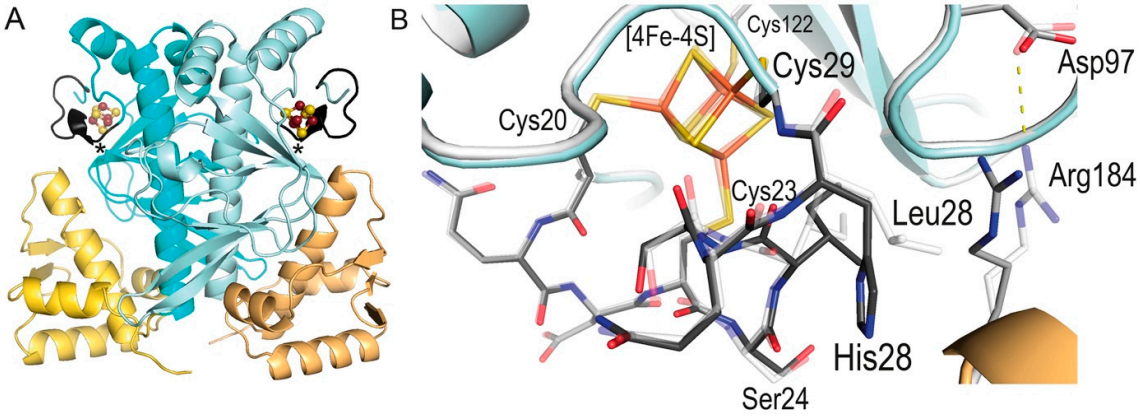


**Figure 7.** Crystallographic characterization of [4Fe-4S] L28H-*Af*FNR. (**A**) Ribbon cartoon of the functional dimer. The N-terminal regions are depicted in cyan and pale cyan using black for the [4Fe-4S] cluster-binding Cys20-Cys29 loops. The His28 mutation site is represented by a star on each monomer. The C-terminal regions are shown in gold and light orange. (**B**) Detail of the Cys20-Cys29 loop and its interaction with the DNA-binding domain, showing the structure of the L28H variant (dark gray C-atoms) superimposed on that of the wt (light gray C atoms) in semi-transparent mode. These figures were made with PyMOL (www.pymol.org, the PyMOL molecular graphics system, version 2.1, Schrödinger, LLC, New York, NY, USA).

An inspection of the region in the structure around the L28H substitution revealed a significant conformational change in the Arg184 side chain (Figure 7B) and a small movement of the DNA-binding domain, which appear to increase its interaction with the Cys20-Cys29 loop of the cluster-binding domain (Figure 7B). In the wt structure, Arg184 makes a salt bridge with Asp97; both of these residues are conserved in *Ec*FNR [54]. The Cys20-Cys29 loop is more ordered in the L28H-*Af*FNR variant than in the 2.65 Å resolution wt structure, especially towards the N-terminal region, as evidenced by a significant increase in the observed electron density. The latter is correlated with a decrease in the temperature factor of the Sγ atoms of Cys20, Cys23 and Cys29 from 145, 132 and 120 $Å^2$ in the wt structure to 100, 95 and 83 $Å^2$ in the L28H variant structure.

### *3.6. MD Simulations of wt and L28H-AfFNR Provide a Possible Explanation for the $O_2$ Resistance Phenotype of the Variant*

The comparison of the wt and L28H-*Af*FNR X-ray structures revealed no significant conformational changes in the Cys20-Cys29 loop and the [4Fe-4S] cluster (Figure 7B). The only clear difference was the shift of Arg184 caused by the change from Leu28 to His28. In the L28H variant, Arg184 and His28 are close to each other but a cation–π interaction is not observed (Figure 7B). Because such an interaction could affect the flexibility of the Cys20-Cys29 loop and contribute to the observed $O_2$-resistant phenotype, a series of MD simulations was carried out to investigate its possible formation in solution. First, a 1 μs simulation of [4Fe-4S] L28H-*Af*FNR indicated that a cation–π interaction could be present.

The radial distribution probability for the interaction between the Cζ of Arg184 and the center of mass of the unprotonated imidazole ring of His28 (Figure 8A) was very similar to the one found for an Arg-His dipeptide [55].

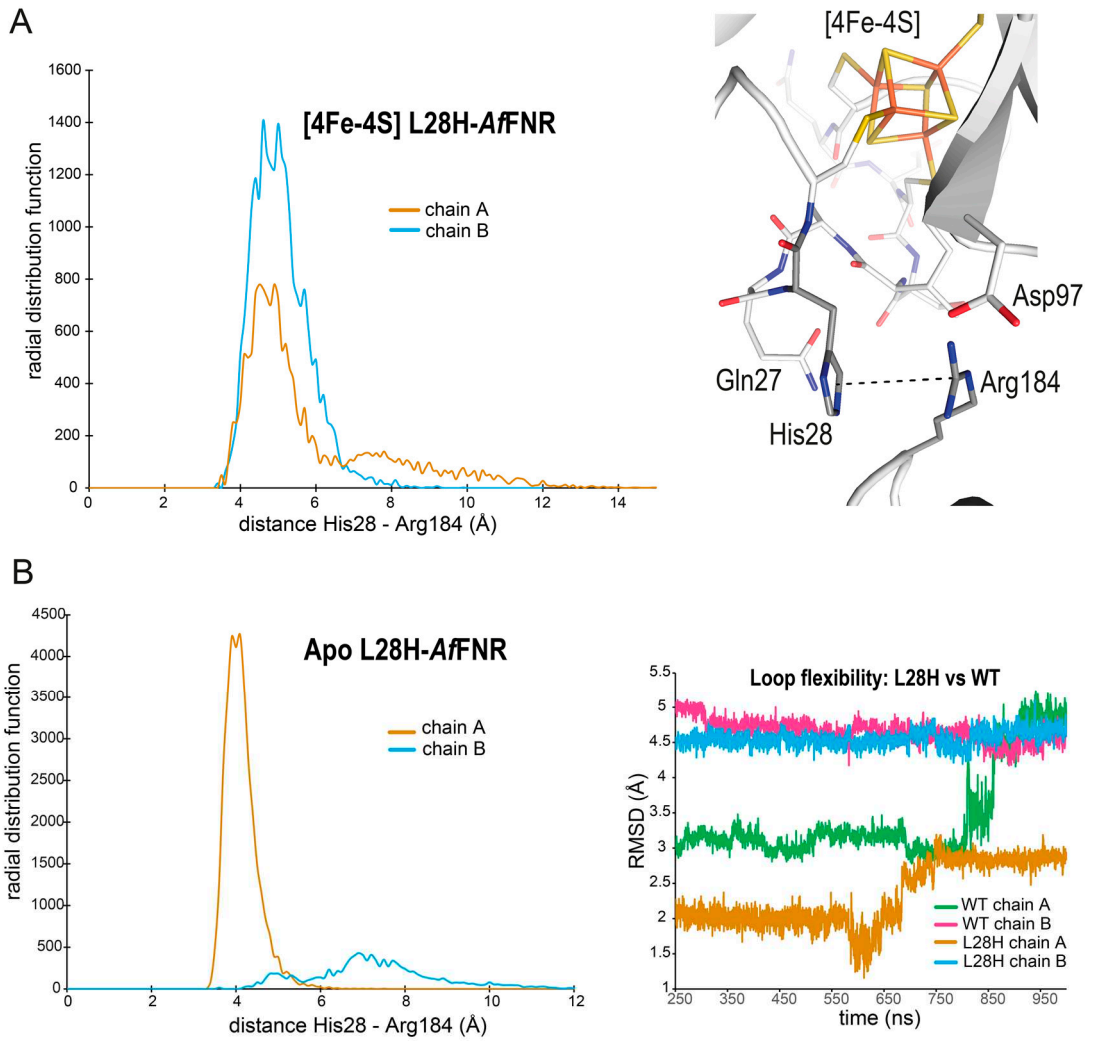


**Figure 8.** MD simulations of L28H-*Af*FNR and comparison to wt *Af*FNR. (**A**) Left panel: radial distribution function (RDF) calculated along the MD simulation of the [4Fe-4S] L28H-*Af*FNR dimer, between the Cζ atom of the Arg184 guanidinium group and the center of mass of the His28 ring. The simulations reveal an asymmetry of dynamics in chain A (orange) and chain B (cyan), most likely arising from interactions between the two monomers. Right panel: cation–π interaction between Arg184 and His28 (indicated by a black dashed line) shown for one of the frames along the MD trajectory of the [4Fe-4S] L28H-*Af*FNR. This type of interaction has been observed with the highest probability at a distance of 4.6 Å in a His-Arg dipeptide [55]. (**B**) Left panel: radial distribution function calculated, along the MD simulation of the apo L28H-*Af*FNR dimer, between the Cζ atom of the Arg184 guanidinium group and the center of mass of the His28 ring of chain A (orange) and chain B (cyan) [55]. The cation–π interaction is present through most of the simulation in chain A (orange line), while it is formed only briefly towards the end of the simulation in chain B (cyan line). Right panel: root mean square deviation (RMSD) of the Cys20-Cys29 loop relative to its conformation in the crystal structure along the dynamics of the apo wt-*Af*FNR (chains A and B in green and pink, respectively) and that of the apo L28H-*Af*FNR (chains A and B in orange and cyan, respectively). The Cys20-Cys29 loop flexibility of the variant (see RMSD) is correlated with the presence of the cation–π interaction (see RDF); the loop is less flexible when the interaction is present (orange lines).

Next, a 1 μs simulation of [4Fe-4S] wt *Af*FNR showed that, with only rare exceptions, the distance between the closest heavy atoms of the Leu28 and Arg184 side chains was kept at 4-to-6 Å, owing to van der Waals interactions (not shown). However, in these two simulations, it was not possible to evaluate the effect of the substitution on the flexibility of the Cys20-Cys29 loop because its three Cys residues are bonded to the cluster (see Methods for details). One way to explore the effect of a possible cation–π interaction on the loop flexibility was to remove the cluster. Although it is obvious that this cannot represent the first step in the reaction of the [4Fe-4S] cluster with $O_2$, it could provide a way to test the influence of that interaction on the intrinsic flexibility of the loop. Indeed, the His28-Arg184 cation–π interaction was also observed without the cluster (Figure 8B). As shown by the root mean square deviations obtained during the 1 μs MD simulation of the apo L28H-*Af*FNR, the Cys20-Cys29 loop is less flexible when the His28-Arg184 cation–π is present than when it is absent (Figure 8B). In addition, it is inherently less flexible than its wt counterpart (Figure 8B).

## 4. Discussion

The FNR proteins of facultative anaerobes act as transcriptional regulators to coordinate the switch between aerobic and anaerobic respiratory growth. In the absence of $O_2$, FNR proteins are homodimers capable of site-specific DNA binding. Each subunit of the FNR dimer possesses a $[4Fe\text{-}4S]^{2+}$ cluster. $O_2$ reacts with these [4Fe-4S] clusters to ultimately (via a series of intermediates) yield monomeric, non-DNA-binding, apo-FNR. In addition to the primary $O_2$ signal, FNR [4Fe-4S] clusters also react with NO, an intermediate in, or by-product of, anaerobic nitrate respiration. This raises important questions of how FNR, and other iron–sulfur cluster-based regulators, discriminate between alternative signaling molecules.

Early attempts to understand the mechanism by which FNR became inactivated led to the discovery of variants that increased the expression of nitrate reductase (*narGHJI*) during aerobic growth conditions [48]. One of these, L28H-*Ec*FNR, possessed a [4Fe-4S] cluster that was relatively stable in air, permitting sufficient homodimeric L28H-*Ec*FNR to persist in the presence of $O_2$, enabling site-specific DNA binding [30]. Here, we confirmed that L28H-*Ec*FNR possesses [4Fe-4S] clusters that are more stable under aerobic conditions compared to the wt protein. Nevertheless, we show that the L28H-*Ec*FNR [4Fe-4S] cluster does react with $O_2$, albeit slowly, resulting in the monomerization and abolition of site-specific DNA binding. Thus, as for the wt protein, the integrity of the [4Fe-4S] cluster is important for L28H-*Ec*FNR to bind target DNA.

Despite its enhanced tolerance to $O_2$, we show that L28H-*Ec*FNR remains acutely susceptible to NO. Overall, the kinetics of the reaction of the variant with NO were broadly similar to those previously reported for wt-*Ec*FNR. Both reacted rapidly with NO (with similar rate constants), in a multiphasic reaction (A → B → C → D → E) that resulted in a dissociation into monomers, with all steps displaying a first-order dependence on NO at lower (physiologically relevant) concentrations [24]. However, differences in the thermodynamic titrations indicated that, while wt-*Ec*FNR reacts in a non-concerted reaction with a likely intermediate at ~4–5 NO molecules per cluster, L28H-*Ec*FNR exhibited a concerted reaction with no evidence of a stable intermediate at this, or any other, NO-to-cluster ratio. Thus, although the L28H substitution had profound effects on the sensitivity of the *Ec*FNR [4Fe-4S] cluster to $O_2$, it had little effect on the NO reactivity.

At the time of writing, there is no high-resolution structural information for *Ec*FNR. However, a 2.65 Å resolution crystal structure of dimeric [4Fe-4S] FNR from the marine bacterium *A. fischeri* (*Af*FNR) has provided a structural framework upon which observations on the *Ec*FNR protein can be interpreted and mechanistic insights can be gained [11,56]. The introduction of the *Af fnr* gene can restore anaerobic respiration on nitrate in an *E. coli fnr*$^-$ mutant, and *Af*FNR shares an 84% amino acid sequence identity with the *E. coli* protein [10,54]. Here, we show that, like its *Ec* counterpart [30], the L28H-*Af*FNR protein reacts with $O_2$ very slowly (Figures S1B and S5). Moreover, the L28H-*Af*FNR crystal struc-

ture described here offers insights into why L28H-FNR variants are resistant to $O_2$, but, as shown for L28H-*Ec*FNR, remain largely unaffected in reactions with NO.

The crystal structure of L28H-*Af*FNR confirmed the conclusion drawn from previous mutagenesis studies, which suggested that the introduced His residue did not act as a cluster ligand [30]. In fact, the L28H substitution results in only one highly localized structural change in *Af*FNR: the shift of the Arg184 side chain (Figure 7B). Although a cation–π interaction between His28 and Arg184 was not observed in the crystal structure (Figure 7B), MD simulations showed that it is likely to be substantial in solution (Figure 8A). To understand why this interaction was not observed in the crystal, the X-ray structure was further examined. We noted that crystal-packing contacts, at both the top of the cluster-binding N-terminal region and the bottom of the DNA-binding region, place His28 and Arg184 too far apart to form a cation–π interaction. However, during the MD solution simulations, these two regions undergo rigid body displacements that bring these residues closer to each other, such that the interaction becomes possible. Furthermore, in simulations where the cluster was removed, it was found that interaction between His28 and Arg184 could significantly restrict the flexibility of the Cys20-Cys29 loop. These observations lead us to suggest the following as a possible explanation for the observed $O_2$-resistant phenotype of the L28H-*Ec*FNR protein.

Previously, it was noted that the electron density associated with the Cys20 thiolate side chain was weak in the wt-*Af*FNR crystal structure, leading to the suggestion that the bond may be naturally strained and the position of the Cys20 side chain could be relatively flexible [11]. The structure of L28H-*Af*FNR reported here indicates that the L28H substitution lowers the conformational flexibility of the Cys20-Cys29 loop, which could, in turn, reduce strain on the Cys20(S)-Fe bond. The effect of this may be to diminish the propensity of the Cys20 thiolate to dissociate from the cluster iron, which, in turn, decreases the rate of iron dissociation from the [4Fe-4S] cluster. The Grenoble group proposed that this process may be necessary in order for a reaction with $O_2$ to occur [11]. In such a model, the outer-sphere reaction of $O_2$ with a transiently formed $[3Fe\text{-}4S]^0$ cluster results in oxidation to an EPR-active $[3Fe\text{-}4S]^{1+}$ form that is the first committed step on the conversion pathway to the $[2Fe\text{-}2S]^{2+}$ monomeric form. Interestingly, the Norwich group recently demonstrated that the iron sensor RirA, a member of the Rrf2 super-family of regulators, exhibits sensitivity to $O_2$ through the reaction of a $[3Fe\text{-}4S]^0$ form that is in equilibrium with a $[4Fe\text{-}4S]^{2+}$ form, but which is favored under low-iron conditions [57]. Thus, the effect of the L28H substitution could be to stabilize the coordination of the Cys20 thiolate to the cluster, and hence dramatically lower the capacity for, and sensitivity to, $O_2$-mediated outer-sphere oxidation processes. Consistent with this, the electron density associated with the thiolate of Cys20 is stronger than observed in the wt *Af*FNR structure. Although the Cys20-Fe bond structurally appears as the best candidate to initiate cluster degradation, we cannot rule out the possibility that the first reaction step could concern either the Cys23-Fe or the Cys29-Fe bonds instead.

In contrast to $O_2$, which can participate in both inner-sphere and outer-sphere redox reactions with metal ions, and favors the outer sphere in reactions with iron–sulfur clusters, NO more commonly reacts with metal ions via inner-sphere processes, modifying the coordination sphere of target metal ions and inducing redox changes [58,59]. Overall, the rapid kinetics reported here for the reaction of L28H-*Ec*FNR with NO are broadly comparable to those of wt-*Ec*FNR. Thus, it appears that the stabilizing effect of the L28H substitution towards $O_2$-mediated outer-sphere processes does not confer protection against inner-sphere NO reactions, probably because the latter do not initially depend on the cleavage of a Cys-Fe bond. However, the reduced conformational flexibility of the Cys20-Cys29 loop in the L28H variant may be important for the observed 50%-reduced rate of the initial reaction with NO, and for the distinct concentration dependencies observed at high NO concentrations. Thus, the decreased conformational flexibility of the Cys20-Cys29 cluster-binding loop imparted via the replacement of Leu28 by His, which we propose inhibits

outer-sphere $O_2$ reactivity, only partially impairs inner-sphere NO reactivity, providing new insights into how iron–sulfur cluster regulators distinguish between $O_2$ and NO.

## 5. Concluding Remarks

In *E. coli* and other enterobacteria, FNR primarily functions as a global $O_2$ sensor that controls the switch between aerobic and anaerobic metabolism. In addition, in the marine bacterium *Aliivibrio fischeri*, it also regulates the $O_2$-dependent luciferin–luciferase reaction [10]. In mechanistic terms, FNR is amongst the best characterized of the iron–sulfur cluster-containing transcriptional regulators, although it is still unclear what controls its sensitivity to $O_2$. FNR is also known to regulate, as a secondary role, gene expression in response to physiological concentrations of NO. Thus, it represents a useful model for better understanding how iron–sulfur cluster regulators discriminate between $O_2$ and NO. Based on our MD simulations, it can be concluded that the main impact of L28H substitution is to stabilize the cluster-binding loop through the formation of a cation–π interaction between His28 and Arg184. The flexibility of this loop appears to be crucial to the outer-sphere reaction of the cluster with $O_2$. It is much less important for inner-sphere reactions with NO, resulting in a greater specificity of L28H FNR towards this gas.

**Supplementary Materials:** The following supporting information can be downloaded at https://www.mdpi.com/article/10.3390/inorganics11120450/s1: Figure S1: Reaction of L28H-*Ec*FNR and L28H-*Af*FNR with O2 monitored by native MS; Figure S2: Deconvolution of EPR spectra res;ulting from nitrosylation of [4Fe-4S] L28H-*Ec*FNR; Figure S3: Gel filtration of [4Fe-4S]- L28H-*Ec*FNR before and after nitrosylation; Figure S4: UV-visible properties of nitrosylated [4Fe-4S] L28H-*Ec*FNR; Figure S5: Reaction of [4Fe-4S]-*Af*FNR with O2; Table S1: X-ray data collection and refinement statistics for [4Fe-4S] L28H-*Af*FNR; Table S2: Rate constants for the nitrosylation of [4Fe-4S] L28H-*Ec*FNR with NO and comparison to wild-type FNR and Wbl proteins. References [24,28,50,60–64] are cited in the supplementary materials.

**Author Contributions:** J.C.C., P.A., E.d.R., J.G., A.V., J.C.F.-C. and N.E.L.B. conceived the study and contributed to the experimental design. J.C.C., C.D. and M.R.S. contributed to the protein production and purification. J.C.C., E.d.R. and A.V. carried out the spectroscopic, kinetic and structural experiments and analyzed the data. P.A. carried out the molecular dynamics simulations and their analyses. J.C.C., P.A., E.d.R., J.G., A.V., J.C.F.-C. and N.E.L.B. wrote the paper with assistance from all authors. All authors have read and agreed to the published version of the manuscript.

**Funding:** This work was supported by the Biotechnology and Biological Sciences Research Council (BBSRC) grant BB/V006851/1 (UK) and grant ANR-18-CE11-0010 from the Agence Nationale pour la Recherche (France).

**Data Availability Statement:** Data supporting the conclusions of this study are available in the main paper, with additional experimental data included in the Supplementary Materials. Atomic coordinates and structure factors for the reported crystal structure have been deposited with the Protein Data Bank (https://www.rcsb.org) under accession number 8QTO.

**Acknowledgments:** We thank Myles Cheesman (UEA) for access to CD and EPR spectrometers and Michael McArthur (Norwich Medical School, UEA) for the kind gift of the Rhodamine Green-labelled *napF* probe. The structural biology applications used in this work were compiled and configured by SBGrid [65].

**Conflicts of Interest:** The authors declare that there are no conflict of interest.

## References

1. Fleischhacker, A.S.; Kiley, P.J. Iron-containing transcription factors and their roles as sensors. *Curr. Opin. Chem. Biol.* **2011**, *15*, 335–341. [CrossRef]
2. Crack, J.C.; Green, J.; Thomson, A.J.; Le Brun, N.E. Iron-sulfur clusters as biological sensors: The chemistry of reactions with molecular oxygen and nitric oxide. *Acc. Chem. Res.* **2014**, *47*, 3196–3205. [CrossRef]
3. Guest, J.R.; Russell, G.C. Complexes and complexities of the citric acid cycle in Escherichia coli. *Curr. Top. Cell Regul.* **1992**, *33*, 231–247.

4. Khoroshilova, N.; Beinert, H.; Kiley, P.J. Association of a polynuclear iron-sulfur center with a mutant FNR protein enhances DNA-binding. *Proc. Natl. Acad. Sci. USA* **1995**, *92*, 2499–2503. [CrossRef]
5. Guest, J.R. The Leeuwenhoek Lecture, 1995. Adaptation to life without oxygen. *Philos. Trans. R. Soc. Lond. B Biol. Sci.* **1995**, *350*, 189–202.
6. Khoroshilova, N.; Popescu, C.; Munck, E.; Beinert, H.; Kiley, P.J. Iron-sulfur cluster disassembly in the FNR protein of *Escherichia coli* by $O_2$: [4Fe-4S] to [2Fe-2S] conversion with loss of biological activity. *Proc. Natl. Acad. Sci. USA* **1997**, *94*, 6087–6092. [CrossRef]
7. Beinert, H.; Kiley, P.J. Fe-S proteins in sensing and regulatory functions. *Curr. Opin. Chem. Biol.* **1999**, *3*, 152–157. [CrossRef]
8. Guest, J.R. Oxygen-regulated gene expression in *Escherichia coli*. The 1992 Marjory Stephenson Prize Lecture. *J. Gen. Microbiol.* **1992**, *138*, 2253–2263. [CrossRef]
9. Dunn, A.K. *Vibrio fischeri* metabolism: Symbiosis and beyond. *Adv. Microb. Physiol.* **2012**, *61*, 37–68.
10. Septer, A.N.; Bose, J.L.; Dunn, A.K.; Stabb, E.V. FNR-mediated regulation of bioluminescence and anaerobic respiration in the light-organ symbiont *Vibrio fischeri*. *FEMS Microbiol. Lett.* **2010**, *306*, 72–81. [CrossRef]
11. Volbeda, A.; Darnault, C.; Renoux, O.; Nicolet, Y.; Fontecilla-Camps, J.C. The crystal structure of the global anaerobic transcriptional regulator FNR explains its extremely fine-tuned monomer-dimer equilibrium. *Sci. Adv.* **2015**, *1*, e1501086. [CrossRef]
12. Green, J.; Guest, J.R. A role for iron in transcriptional activation by FNR. *FEBS Lett.* **1993**, *329*, 55–58. [CrossRef]
13. Green, J.; Irvine, A.S.; Meng, W.; Guest, J.R. FNR-DNA interactions at natural and semi-synthetic promoters. *Mol. Microbiol.* **1996**, *19*, 125–137. [CrossRef]
14. Kiley, P.J.; Beinert, H. Oxygen sensing by the global regulator, FNR: The role of the iron-sulfur cluster. *FEMS Microbiol. Revs.* **1999**, *22*, 341–352. [CrossRef]
15. Lazazzera, B.A.; Bates, D.M.; Kiley, P.J. The activity of the *Escherichia coli* transcription factor FNR is regulated by a change in oligomeric state. *Genes Dev.* **1993**, *7*, 1993–2005. [CrossRef]
16. Crack, J.C.; Gaskell, A.A.; Green, J.; Cheesman, M.R.; Le Brun, N.E.; Thomson, A.J. Influence of the environment on the $[4Fe\text{-}4S]^{2+}$ to $[2Fe\text{-}2S]^{2+}$ cluster switch in the transcriptional regulator FNR. *J. Am. Chem. Soc.* **2008**, *130*, 1749–1758. [CrossRef]
17. Crack, J.C.; Green, J.; Cheesman, M.R.; Le Brun, N.E.; Thomson, A.J. Superoxide-mediated amplification of the oxygen-induced switch from [4Fe-4S] to [2Fe-2S] clusters in the transcriptional regulator FNR. *Proc. Natl. Acad. Sci. USA* **2007**, *104*, 2092–2097. [CrossRef]
18. Crack, J.C.; Thomson, A.J.; Le Brun, N.E. Mass spectrometric identification of intermediates in the $O_2$-driven [4Fe-4S] to [2Fe-2S] cluster conversion in FNR. *Proc. Natl. Acad. Sci. USA* **2017**, *114*, E3215–E3223. [CrossRef]
19. Popescu, C.V.; Bates, D.M.; Beinert, H.; Munck, E.; Kiley, P.J. Mössbauer spectroscopy as a tool for the study of activation/inactivation of the transcription regulator FNR in whole cells of *Escherichia coli*. *Proc. Natl. Acad. Sci. USA* **1998**, *95*, 13431–13435. [CrossRef]
20. Vine, C.E.; Cole, J.A. Unresolved sources, sinks, and pathways for the recovery of enteric bacteria from nitrosative stress. *FEMS Microbiol. Lett.* **2011**, *325*, 99–107. [CrossRef]
21. Nunoshiba, T.; deRojas-Walker, T.; Wishnok, J.S.; Tannenbaum, S.R.; Demple, B. Activation by nitric oxide of an oxidative-stress response that defends *Escherichia coli* against activated macrophages. *Proc. Natl. Acad. Sci. USA* **1993**, *90*, 9993–9997. [CrossRef]
22. Cruz-Ramos, H.; Crack, J.; Wu, G.G.; Hughes, M.N.; Scott, C.; Thomson, A.J.; Green, J.; Poole, R.K. NO sensing by FNR: Regulation of the *Escherichia coli* NO-detoxifying flavohaemoglobin, Hmp. *EMBO J.* **2002**, *21*, 3235–3244. [CrossRef]
23. Pullan, S.T.; Gidley, M.D.; Jones, R.A.; Barrett, J.; Stevanin, T.A.; Read, R.C.; Green, J.; Poole, R.K. Nitric oxide in chemostat-cultured *Escherichia coli* is sensed by Fnr and other global regulators: Unaltered methionine biosynthesis indicates lack of S nitrosation. *J. Bacteriol.* **2007**, *189*, 1845–1855. [CrossRef]
24. Crack, J.C.; Stapleton, M.R.; Green, J.; Thomson, A.J.; Le Brun, N.E. Mechanism of $[4Fe\text{-}4S](Cys)_4$ cluster nitrosylation is conserved among NO-responsive regulators. *J. Biol. Chem.* **2013**, *288*, 11492–11502. [CrossRef]
25. Crack, J.C.; Munnoch, J.; Dodd, E.L.; Knowles, F.; Al Bassam, M.M.; Kamali, S.; Holland, A.A.; Cramer, S.P.; Hamilton, C.J.; Johnson, M.K.; et al. NsrR from *Streptomyces coelicolor* is a nitric oxide-sensing [4Fe-4S] cluster protein with a specialized regulatory function. *J. Biol. Chem.* **2015**, *290*, 12689–12704. [CrossRef]
26. Partridge, J.D.; Bodenmiller, D.M.; Humphrys, M.S.; Spiro, S. NsrR targets in the *Escherichia coli* genome: New insights into DNA sequence requirements for binding and a role for NsrR in the regulation of motility. *Mol. Microbiol.* **2009**, *73*, 680–694. [CrossRef]
27. Mukhopadhyay, P.; Zheng, M.; Bedzyk, L.A.; LaRossa, R.A.; Storz, G. Prominent roles of the NorR and Fur regulators in the *Escherichia coli* transcriptional response to reactive nitrogen species. *Proc. Natl. Acad. Sci. USA* **2004**, *101*, 745–750. [CrossRef]
28. Crack, J.C.; Smith, L.J.; Stapleton, M.R.; Peck, J.; Watmough, N.J.; Buttner, M.J.; Buxton, R.S.; Green, J.; Oganesyan, V.S.; Thomson, A.J.; et al. Mechanistic insight into the nitrosylation of the [4Fe-4S] cluster of WhiB-like proteins. *J. Am. Chem. Soc.* **2011**, *133*, 1112–1121. [CrossRef]
29. Jervis, A.J.; Crack, J.C.; White, G.; Artymiuk, P.J.; Cheesman, M.R.; Thomson, A.J.; Le Brun, N.E.; Green, J. The $O_2$ sensitivity of the transcription factor FNR is controlled by Ser24 modulating the kinetics of [4Fe-4S] to [2Fe-2S] conversion. *Proc. Natl. Acad. Sci. USA* **2009**, *106*, 4659–4664. [CrossRef]
30. Bates, D.M.; Popescu, C.V.; Khoroshilova, N.; Vogt, K.; Beinert, H.; Munck, E.; Kiley, P.J. Substitution of leucine 28 with histidine in the *Escherichia coli* transcription factor FNR results in increased stability of the $[4Fe\text{-}4S]^{2+}$ cluster to oxygen. *J. Biol. Chem.* **2000**, *275*, 6234–6240. [CrossRef]

31. Bradford, M.M. A rapid and sensitive method for the quantitation of microgram quantities of protein utilizing the principle of protein-dye binding. *Anal. Biochem.* **1976**, *72*, 248–254. [CrossRef]
32. Beinert, H. Semi-micro methods for analysis of labile sulfide and of labile sulfide plus sulfane sulfur in unusually stable iron-sulfur proteins. *Anal. Biochem.* **1983**, *131*, 373–378. [CrossRef]
33. Kabsch, W. XDS. *Acta Crystallogr. D Biol. Crystallogr.* **2010**, *66*, 125–132. [CrossRef]
34. Evans, P.R.; Murshudov, G.N. How good are my data and what is the resolution? *Acta Crystallogr. D Biol. Crystallogr.* **2013**, *69*, 1204–1214. [CrossRef]
35. McCoy, A.J.; Grosse-Kunstleve, R.W.; Adams, P.D.; Winn, M.D.; Storoni, L.C.; Read, R.J. Phaser crystallographic software. *J. Appl. Crystallogr.* **2007**, *40*, 658–674. [CrossRef]
36. Murshudov, G.N.; Skubak, P.; Lebedev, A.A.; Pannu, N.S.; Steiner, R.A.; Nicholls, R.A.; Winn, M.D.; Long, F.; Vagin, A.A. REFMAC5 for the refinement of macromolecular crystal structures. *Acta Crystallogr. D Biol. Crystallogr.* **2011**, *67*, 355–367. [CrossRef]
37. Adams, P.D.; Afonine, P.V.; Bunkoczi, G.; Chen, V.B.; Davis, I.W.; Echols, N.; Headd, J.J.; Hung, L.W.; Kapral, G.J.; Grosse-Kunstleve, R.W.; et al. PHENIX: A comprehensive Python-based system for macromolecular structure solution. *Acta Crystallogr. D Biol. Crystallogr.* **2010**, *66*, 213–221. [CrossRef]
38. Emsley, P.; Lohkamp, B.; Scott, W.G.; Cowtan, K. Features and development of Coot. *Acta Crystallogr. D Biol. Crystallogr.* **2010**, *66*, 486–501. [CrossRef]
39. Kuzmic, P. Program DYNAFIT for the analysis of enzyme kinetic data: Application to HIV proteinase. *Anal. Biochem.* **1996**, *237*, 260–273. [CrossRef]
40. Lewis, R.S.; Deen, W.M. Kinetics of the reaction of nitric oxide with oxygen in aqueous solutions. *Chem. Res. Toxicol.* **1994**, *7*, 568–574. [CrossRef]
41. Saavedra, J.E.; Southan, G.J.; Davies, K.M.; Lundell, A.; Markou, C.; Hanson, S.R.; Adrie, C.; Hurford, W.E.; Zapol, W.M.; Keefer, L.K. Localizing antithrombotic and vasodilatory activity with a novel, ultrafast nitric oxide donor. *J. Med. Chem.* **1996**, *39*, 4361–4365. [CrossRef]
42. Keefer, L.K.; Nims, R.W.; Davies, K.M.; Wink, D.A. "NONOates" (1-substituted diazen-1-ium-1,2-diolates) as nitric oxide donors: Convenient nitric oxide dosage forms. *Meth. Enzymol.* **1996**, *268*, 281–293.
43. *Schrödinger Release 2023-1*; Schrödinger, LLC: New York, NY, USA, 2023.
44. Mouesca, J.M.; Chen, J.L.; Noodleman, L.; Bashford, D.; Case, D.A. Density-functional Poisson-Boltzmann calculations of redox potentials for iron-sulfur clusters. *J. Am. Chem. Soc.* **1994**, *116*, 11898–11914. [CrossRef]
45. Lu, C.; Wu, C.J.; Ghoreishi, D.; Chen, W.; Wang, L.L.; Damm, W.; Ross, G.A.; Dahlgren, M.K.; Russell, E.; Von Bargen, C.D.; et al. OPLS4: Improving force field accuracy on challenging regimes of chemical space. *J. Chem. Theory Comput.* **2021**, *17*, 4291–4300. [CrossRef]
46. Jorgensen, W.L.; Chandrasekhar, J.; Madura, J.D.; Impey, R.W.; Klein, M.L. Comparison of simple potential functions for simulating liquid water. *J. Chem. Phys.* **1983**, *79*, 926–935. [CrossRef]
47. Schrödinger. *Maestro, Desmond-Interoperability Tools*; Schrödinger: New York, NY, USA, 2019.
48. Kiley, P.J.; Reznikoff, W.S. FNR mutants that activate gene expression in the presence of oxygen. *J. Bacteriol.* **1991**, *173*, 16–22. [CrossRef]
49. Vasilieva, S.V.; Streltsova, D.A.; Vlaskina, A.V.; Mikoian, V.D.; Vanin, A.F. Sources of divalent sulfur allow recovery of the Fnr $[4Fe\text{-}4S]^{2+}$ center in *Escherichia coli* incubated with nitric oxide donors. *Biophysics* **2012**, *57*, 166–169. [CrossRef]
50. Frolov, E.N.; Vanin, A.F. New type of paramagnetic nitrosyl complexes of non-heme iron. *Biofizika* **1973**, *18*, 605–610.
51. Lazazzera, B.A.; Beinert, H.; Khoroshilova, N.; Kennedy, M.C.; Kiley, P.J. DNA binding and dimerization of the Fe-S-containing FNR protein from *Escherichia coli* are regulated by oxygen. *J. Biol. Chem.* **1996**, *271*, 2762–2768. [CrossRef]
52. Smith, A.D.; Agar, J.N.; Johnson, K.A.; Frazzon, J.; Amster, I.J.; Dean, D.R.; Johnson, M.K. Sulfur transfer from IscS to IscU: The first step in iron-sulfur cluster biosynthesis. *J. Am. Chem. Soc.* **2001**, *123*, 11103–11104. [CrossRef]
53. Zhang, B.; Crack, J.C.; Subramanian, S.; Green, J.; Thomson, A.J.; Le Brun, N.E.; Johnson, M.K. Reversible cycling between cysteine persulfide-ligated [2Fe-2S] and cysteine-ligated [4Fe-4S] clusters in the FNR regulatory protein. *Proc. Natl. Acad. Sci. USA* **2012**, *109*, 15734–15739. [CrossRef]
54. Volbeda, A.; Nicolet, Y.; Fontecilla-Camps, J.C. Fumarate and nitrate reduction regulator (FNR). In *Encyclopedia of Inorganic and Bioinorganic Chemistry*; Wiley: Hoboken, NJ, USA, 2017.
55. Heyda, J.; Mason, P.E.; Jungwirth, P. Attractive interactions between side chains of histidine-histidine and histidine-arginine-based cationic dipeptides in water. *J. Phys. Chem. B* **2010**, *114*, 8744–8749. [CrossRef]
56. Mettert, E.L.; Kiley, P.J. Reassessing the structure and function relationship of the $O_2$ sensing transcription factor FNR. *Antiox. Redox Signal.* **2018**, *29*, 1830–1840. [CrossRef]
57. Pellicer Martinez, M.T.; Crack, J.C.; Stewart, M.Y.; Bradley, J.M.; Svistunenko, D.A.; Johnston, A.W.; Cheesman, M.R.; Todd, J.D.; Le Brun, N.E. Mechanisms of iron- and $O_2$-sensing by the [4Fe-4S] cluster of the global iron regulator RirA. *Elife* **2019**, *8*, e47804. [CrossRef]
58. Butler, A.R.; Glidewell, C.; Li, M. Nitrosyl complexes of iron-sulfur clusters. *Adv. Inorg. Chem.* **1988**, *32*, 335–393.
59. Bruckdorfer, R. The basics about nitric oxide. *Mol. Aspects Med.* **2005**, *26*, 3–31. [CrossRef]

60. Bryar, T.R.; Eaton, D.R. Electronic configuration and structure of paramagnetic iron dinitrosyl complexes. *Can. J. Chem.* **1992**, *70*, 1917–1926. [CrossRef]
61. Costanzo, S.; Menage, S.; Purrello, R.; Bonomo, R.P.; Fontecave, M. Re-examination of the formation of dinitrosyl-iron complexes during reaction of S-nitrosothiols with Fe(II). *Inorg. Chim. Acta* **2001**, *318*, 1–7. [CrossRef]
62. Kim, S.O.; Orii, Y.; Lloyd, D.; Hughes, M.N.; Poole, R.K. Anoxic function for the Escherichia coli flavohaemoglobin (Hmp): Reversible binding of nitric oxide and reduction to nitrous oxide. *FEBS Lett.* **1999**, *445*, 389–394. [CrossRef]
63. Pieper, G.M.; Halligan, N.L.; Hilton, G.; Konorev, E.A.; Felix, C.C.; Roza, A.M.; Adams, M.B.; Griffith, O.W. Non-heme iron protein: A potential target of nitric oxide in acute cardiac allograft rejection. *Proc. Natl. Acad. Sci. USA* **2003**, *100*, 3125–3130. [CrossRef]
64. Williams, C.J.; Headd, J.J.; Moriarty, N.W.; Prisant, M.G.; Videau, L.L.; Deis, L.N.; Verma, V.; Keedy, D.A.; Hintze, B.J.; Chen, V.B.; et al. MolProbity: More and better reference data for improved all-atom structure validation. *Prot. Sci.* **2018**, *27*, 293–315. [CrossRef]
65. Morin, A.; Eisenbraun, B.; Key, J.; Sanschagrin, P.C.; Timony, M.A.; Ottaviano, M.; Sliz, P. Collaboration gets the most out of software. *Elife* **2013**, *2*, e01456. [CrossRef]